Floodwater impacts on residential areas in floodplain areas along Day River system in emergency situation

ANH, Sai Hong
Laboratory of Water Environment Engineering, Division of Bioproduction Environmental Sciences, Department of Agro-environmental Sciences, Graduate School of Bioresource and Bioenvironmental Sciences, Kyushu University

TABATA, Toshinori
Department of Agro-environmental Sciences, Faculty of Agriculture, Kyushu University

HIRAMATSU, Kazuaki
Department of Agro-environmental Sciences, Faculty of Agriculture, Kyushu University

SON, Le Viet
Division of Water Resources Planning for the North Region, Institute of Water Resources Planning

他

https://doi.org/10.5109/4363555

出版情報：九州大学大学院農学研究院紀要. 66 (1), pp.77-90, 2021-03-01. Faculty of Agriculture, Kyushu University
バージョン：
権利関係：

J. Fac. Agr., Kyushu Univ., **66** (1), 77–90 (2021)

Floodwater impacts on residential areas in floodplain areas along Day River system in emergency situation

Sai Hong ANH[1,3], Toshinori TABATA*, Kazuaki HIRAMATSU, Le Viet SON[2] and Masayoshi HARADA

Laboratory of Water Environment Engineering
Division of Bioproduction Environmental Sciences,Department of Agro-environmental Sciences,
Faculty of Agriculture, Kyushu University, Fukuoka 819-0395, Japan
(*Received October 30, 2020 and accepted November 4, 2020*)

Hanoi, the capital of Vietnam, is protected from floods by dike systems for the Red and Day Rivers. In emergency situations resulting from catastrophic floods, floodwater from the Red River is discharged into the Van Coc Lake, which is a regulating reservoir that drains into the Day River system through the Day Weir at the downstream end of the Van Coc Lake. The authors investigated the flood mitigation function of the Van Coc Lake and identified an optimal operation scenario for the lake for the largest recorded flood, which occurred between the 16th and 27th of August 1971. However, a comprehensive evaluation of the flood risk level in residential areas within the floodplain areas located along the Day River system to determine an optimal operation scenario has not been conducted. In this study, a two–dimensional depth-integrated hydrodynamic model was employed to investigate flood risk levels in these residential areas when the floodwater level reached 11.0 m, 12.0 m, and 12.72 m (the flood peak) at the Day Weir and at 10 and 30 h after the flood peak, under the optimal operation scenario. The time at which floodwater from the Van Coc Lake reached the Day Weir was referred to as Time–0 in this study and was used to estimate the movement of floodwater. The study area, from the Day Weir to the downstream end, was more than 100 km in length and was divided into three zones: the northern part, designated Zone 1; the central part, designated Zone 2; and the downstream end part, designated Zone 3. The simulation results were used to produce reliable flood susceptibility maps that identify the areas at greatest risk of being impacted by floodwater. At the flood peak time, residential areas in the study area were inundated at levels of 84.00% (9.50 km^2) in Zone 1, 71.84% (29.18 km^2) in Zone 2, and 98.59% (13.31 km^2) in Zone 3. Floodwater needed 75, 87, and 135 h from Time–0 to reach 11.0 m, 12.0 m, and the flood peak at 12.72 m at the Day Weir. The results of this study form a basis for future land planning and the design of risk reduction strategies for the Day River system and serve as a strong warning about the dangers of floodwater throughout the study area.

Key words: flood hazard mapping, flood risk level, greatest recorded flood, two–dimensional depth–integrated model.

INTRODUCTION

Flooding is a serious issue in cities in developing countries because of the scale of hazard it poses for inhabitants and infrastructure (Nur and Shrestha, 2017). Floods are the most frequent type of natural disaster in the world, and the danger of floods and their terrible consequences have been recorded worldwide. In Vietnam, numerous flood disasters have occurred in recent decades. As shown in Fig. 1, the capital city of Hanoi is located in the Red River Delta in Vietnam. As with most regions in northern Vietnam, Hanoi is directly affected by the hot and humid climate of the Pacific and Indian Oceans. Therefore, it is frequently influenced by massive rainfall events and serious floods (Vietnamese Government, 2005; Anh *et al*., 2020a). Vietnam has been identified as one of the five worst–affected countries by climate change, and Hanoi is located in an area severely affected by climate change. In recent decades, many massive rainfall events have been recorded in the Red River Delta, and flooding in the delta has been a severe problem (AHA–JICA, 2015). The delta has been facing challenges from natural disasters such as floods, drought, and salinization, especially in the context of climate change and sea level rise (MONRE, 2012). In the last 50 years, floods have significantly impacted Hanoi, causing serious damage to homes, possessions, and people (AHA–JICA, 2015). In 1971, there was a severe flood disaster documented in the Red River Delta that caused massive damage to millions of people and dike failures in numerous places and resulted in huge restoration costs. Approximately 100,000 people died during this disaster (NOAA, 1993; Vietnamese Government, 2005). Flood risk management in developing countries is understudied, and flood risk management measures are typically lacking or inadequately implemented (Nkwunonwo *et al*., 2020). Therefore, research on flood risk management in developing countries such as Vietnam is more critical than ever.

According to the European Commission, a prerequisite for effective and efficient flood risk management is in–depth knowledge of the prevailing hazards and risks throughout a river basin and areas of flood risk (European Commission, 2007). Recently, the U.S.

[1] Laboratory of Water Environment Engineering, Division of Bioproduction Environmental Sciences, Department of Agro–environmental Sciences, Graduate School of Bioresource and Bioenvironmental Sciences, Kyushu University
[3] Division of Water Resources Planning for the North Region, Institute of Water Resources Planning, 162A–Tran Quang Khai, Hoan Kiem, Hanoi, Vietnam
* Corresponding author. E–mail: ttabata@bpes.kyushu-u.ac.jp

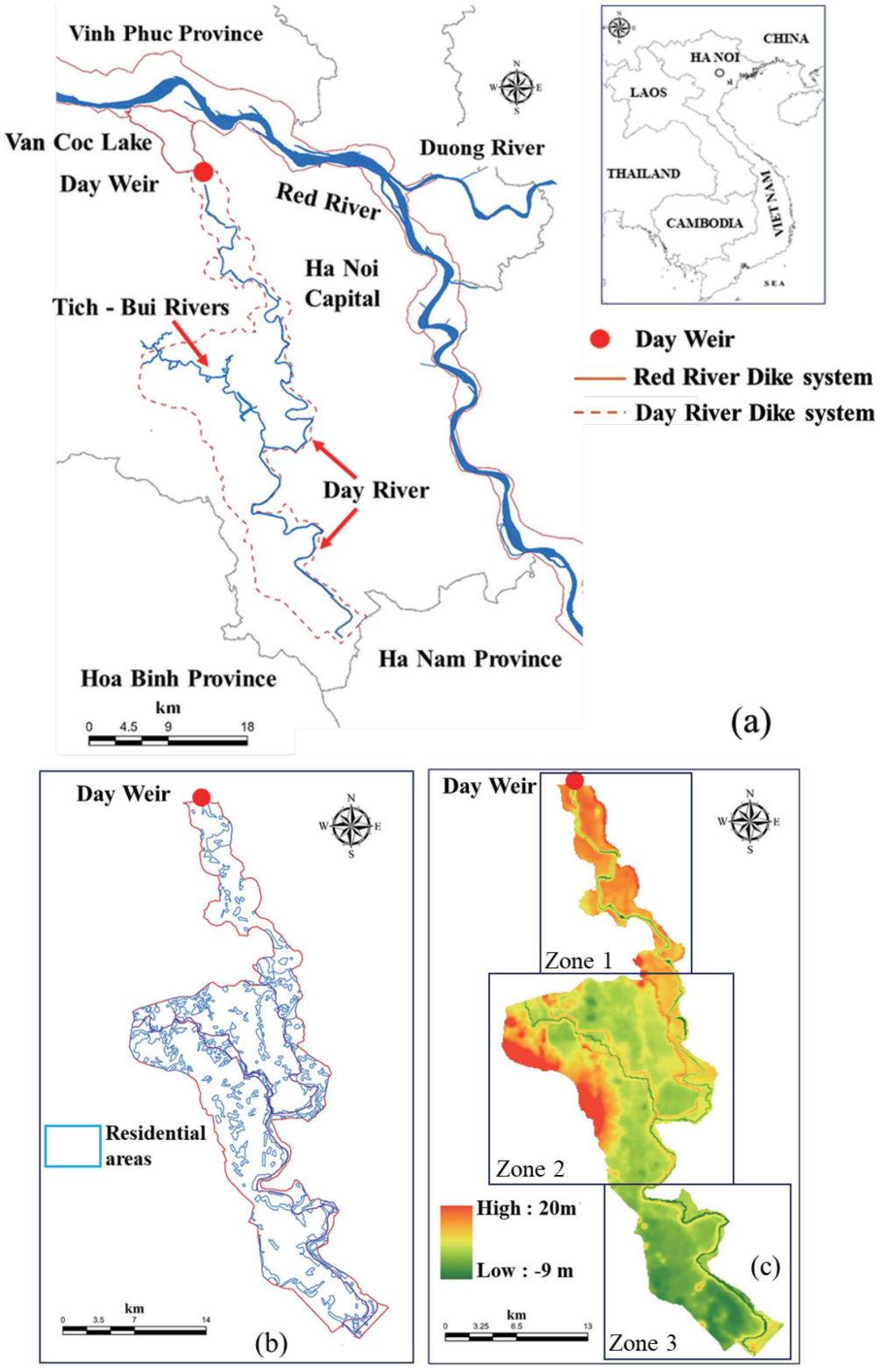

Fig. 1. Schematic diagrams of the study area (a), the residential areas (b), the elevation (c), and Zones 1, 2 and 3.

National Research Council stated that a key to informed decision making on flood risk management is the accurate assessment of risk (National Research Council, 2015). A clear understanding of flood risks is necessary to determine the type and scale of appropriate actions to be taken to avoid, mitigate, transfer, share, or accept flood risks. Flood hazard maps are indispensable tools for displaying information about hazards, vulnerabilities, and risks in a particular area, and they play a very important role in this process (European Commission, 2007).

In recent studies, flood hazard maps have been shown to be a core component of flood risk management for risk assessment and design of mitigation measures in flood–prone areas, even on a global scale (Dottori *et al.*, 2016; Guerriero *et al.*, 2020; Thapa *et al.*, 2020; Shadmehri Toosi *et al.*, 2020; Eini *et al.*, 2020). Many recently studies have utilized flood hazard maps in flood risk management strategies (Hussein *et al.*, 2019; Ogato *et al.*, 2020; Guerriero *et al.*, 2020; Gusain *et al.*, 2020; Costabile *et al.*, 2020; Mishra and Sinha, 2020).

The use of hydrodynamic models of rivers with floodplains is a well–established approach to conducting flood risk analysis (Costabile *et al.*, 2020). There are several popular numerical models for simulating flooding phenomena, including one–dimensional (1–D), two–dimensional (2–D), and three–dimensional (3–D) models (Pinos and Timbe, 2019; Costabile *et al.*, 2020). 1–D models, which are often used to study the effects of flood propagation on rivers and to estimate flow velocities, water levels, and discharges, are typically based on an assumption that water moves only longitudinally in the direction of a river (Liu and Merwade, 2018; Pinos and Timbe, 2019; Fleischmann *et al.*, 2019; Singh *et al.*, 2020). Although 1–D models are still in widespread use, it is likely that the results of a 1–D model will deviate too far from reality for a complex river system (Pinos and Timbe, 2019). They also cannot be used to model channels or situations in which water moves both longitudinally and laterally, which are better represented by 2–D models. For a floodplain with a complex topography, a 2 D model is considered to permit a better representation of the flood path, and horizontal dimensions predominating over vertical dimensions can lead to a more realistic description of the floodplain. (Costabile *et al.*, 2020; Pinos and Timbe, 2019). Furthermore, with the rapid advance of computer technology and the increasing availability of digital elevation models (DEMs), 2–D models have become increasingly widely used to model flows in floodplains, lakes, rivers, and coastal regions (Hu and Kot, 1997; Mignot *et al.*, 2006; Liang *et al.*, 2007; Sun *et al.*, 2008; El Kadi Abderrezzak *et al.*, 2009; Liu *et al.*, 2014; Caviedes–Voullième *et al.*, 2014; An *et al.*, 2015; Bellos and Tsakiris, 2015; Hu *et al.*, 2017; Rollason *et al.*, 2018; Pinos and Timbe, 2019; Haque *et al.*, 2020). 3–D models, which can also represent vertical flows, have recently been used to assess flows in rivers, lakes, and coastal areas (Blumberg and Mellor, 1987; Casulli and Cattani, 1994; Kang and Sotiropoulos, 2012; Marsooli *et al.*, 2016; Rong *et al.*, 2020). However, they have rarely been used for flood hazard assessment because of their complexity, their cost, and the amount of time they require to analyze a large study area (World Bank Group, 2016; Wu and Lin, 2015). In addition, if the study area includes rivers and large floodplains, as is the case for the study area considered in this study, the horizontal flows will typically be much larger than the vertical flows over the major part of the floodplain when floodwater flows into the area (Anh *et al.*, 2020a). Therefore, in this study, a 2–D depth-integrated model was built to simulate the floodwater behavior in the area.

As shown in Fig. 1, the Day River is the main sub–river of the Red River, which is the largest river in northern Vietnam. The Day River runs Hanoi and flows into the East Sea. The Tich–Bui rivers, which also flow through Hanoi, flow into the Day River at Ba Tha, a village in the Ung Hoa District. In emergency situations resulting from catastrophic floods, Hanoi is protected by the Red and Day River dike systems. Floodwater from the Red River is discharged into the Van Coc Lake, which is a regulating reservoir that is located in the Dan Phuong and Phuc Tho Districts and drains into the Day River system through the Day Weir. The floodplain areas and areas protected from floodwater are also shown in Fig. 1. Unfortunately, many large residential areas are located inside the floodplain because of rapid urbanization that has occurred in Hanoi during the last few decades. These residential areas are highly vulnerable to damage during flood emergencies. It is essential to be able to predict the degree and extent of vulnerability of residential areas in the flood plain as part of the flood risk management for these residential areas.

An effective operating procedure for the largest recorded flood to have occurred in the area, between the 16th and 27th of August 1971, which optimized the inflow discharge into the Van Coc Lake as well as the outflow discharge at the Day Weir, was proposed by Anh *et al.* (2020a). In that research, the safety of the operating system of the Van Coc Lake was considered comprehensively by optimizing the inflow discharge at the Van Coc Gate, the overflow point, and the outflow discharge at the Day Weir to protect Hanoi from Red River flood disasters. However, an assessment of the impact of floodwater on the residential areas located in the floodplain areas along the Day River system, which is the downstream area of the Day Weir, has not been conducted for flood events. Therefore, the development of a flood hazard map is indispensable for improving future flood risk planning for critical residential areas in the floodplain area.

In this study, the impact of floodwater during the flood peak on residential areas within the floodplain area in the case of implementation of an effective operating procedure for the largest recorded flood was assessed by numerical simulation. A 2–D depth–integrated hydrodynamic model, combined with the latest DEM, was used to obtain accurate simulation results. The model was validated in several previous studies (Anh *et al.*, 2019; 2020a, 2020b). The input water level boundary condition for the effective operating procedure in an emergency situation, as proposed by (Anh *et al.*, 2020a), was utilized at the Day Weir.

MATERIALS AND METHODS

Study area

Figure 1 shows the location of the study area, residential areas within the floodplain, and an elevation map of the areas from the Day Weir to the downstream end. The study area covered 376.62 km^2 and comprised 150,648 grid cells at a resolution of 50 m. Because the

study area covered a length of more than 100 km from the Day Weir to the downstream end, it was divided into three zones to assess the characteristics of the study area and the simulation results in more detail: Zone 1 in the northern part, Zone 2 in the middle part, and Zone 3 at the downstream end of the study area, as shown in Fig. 1. The elevation of the floodplain areas decreases from north to south in Zone 1, and the elevation in Zone 2 decreases from west to east. In Zone 3, the elevation decreases from north to south. The latest DEM surveys, conducted in 2011 and 2013 by the Institute of Water Resources Planning of the Ministry of Agriculture and Rural Development, Vietnam, were utilized in this study.

Hydrodynamic model and boundary conditions

The study area is a floodplain, and this study focused on the behavior of floodwater, in which horizontal velocities are far greater than vertical velocities. Therefore, a two–dimensional depth–integrated model was used to simulate the behavior of the floodwater in the study area. The shallow water equations used in this study are as follows:

Continuity equation:

$$\frac{\partial \eta}{\partial t}+\frac{\partial}{\partial x}\{U(h+\eta)\}+\frac{\partial}{\partial y}\{V(h+\eta)\}=0 \quad (1)$$

Momentum equations in the x and y directions

$$\frac{\partial U}{\partial t}+U\frac{\partial U}{\partial x}+V\frac{\partial U}{\partial y}=fV-g\frac{\partial \eta}{\partial x}+\upsilon_h\left(\frac{\partial^2 U}{\partial x^2}+\frac{\partial^2 U}{\partial y^2}\right)-\frac{gn^2U\sqrt{U^2+V^2}}{(h+\eta)^{4/3}} \quad (2)$$

$$\frac{\partial V}{\partial t}+U\frac{\partial V}{\partial x}+V\frac{\partial V}{\partial y}=-fU-g\frac{\partial \eta}{\partial y}+\upsilon_h\left(\frac{\partial^2 V}{\partial x^2}+\frac{\partial^2 V}{\partial^2 y}\right)-\frac{gn^2V\sqrt{U^2+V^2}}{(h+\eta)^{4/3}} \quad (3)$$

where U and V are the depth–averaged horizontal velocity components in the x and y directions (m/s), η is the water level (m), t is the time (s), h is the elevation (m), f is the Coriolis force (s^{-1}), g is the gravitational acceleration (m/s^2), n is Manning's coefficient of roughness ($s/m^{1/3}$), and υ_h is the coefficient of eddy viscosity (m^2/s). This coefficient for local flow structures is used in one of the most celebrated subgrid–scale models for eddy viscosity proposed by Smagorinsky (1963). The Smagorinsky turbulent model allows a better presentation of non–uniform velocity in a floodplain and in transition regions between plain and main channels (Lin *et al*., 2008; Ahmadi *et al*., 2009; Pham Van *et al*., 2014). Many studies have utilized the coefficient of eddy viscosity from the Smagorinsky model in calculations of complex turbulent flows (Tejada–Martínez *et al*., 2009; Rakowsky *et al*., 2013; Chacón Rebollo *et al*., 2014; Werren *et al*., 2016; Marras *et al*., 2018). The value of the coefficient of eddy viscosity υ_h was calculated in this study as follows, using the Smagorinsky model (1963):

$$\upsilon_h=\frac{1}{2}S_m A_G\left\{\left(\frac{\partial U}{\partial x}\right)^2+\frac{1}{2}\left(\frac{\partial V}{\partial x}+\frac{\partial U}{\partial y}\right)+\left(\frac{\partial V}{\partial y}\right)^2\right\}^{1/2} \quad (4)$$

where S_m is the Smagorinsky coefficient and A_G is the area of each mesh point (m^2).

The basic parameters are defined as follows: temporal discretization Δt=2.0 s, special discretization Δx=Δy=50 m, S_m=0.2, A_G=$\Delta x\times\Delta y$=2500 m^2, f=5.24×10^{-5} s^{-1}, and g=9.8 m/s^2. Manning's coefficient of roughness n for each grid element was set to be n=0.025 $s/m^{1/3}$–0.172 $s/m^{1/3}$, depending on the vegetation, obstructions, and residential areas. The leapfrog finite difference method was used to calculate the products of the governing equations for the staggered mesh system. The model was run with a time step of Δt=2.0 s, with the water level and velocity calculated alternately.

The wetting and drying processes in the hydrodynamic model are very important because they illustrate the movement of flow from a wet point to a dry point in the area and vice versa. This is very common in seas, closed water bodies, and floodplain areas. The consideration of wetting and drying processes affects the accuracy of the simulation results, and an inadequate treatment of wet and dry fronts in a complex topography can result in important numerical errors (Brufau *et al*., 2004). In recent decades, many methods for modeling wetting and drying processes have been proposed. The first implicit model for handling intertidal flats appears to have been the pioneering model by Leendertse (1970). According to Balzano (1998), other models have been proposed by Benqué *et al*. (1982), Stelling (1984), Falconer and Owens (1987), and Molinaro *et al*. (1994). In this study, the study area was a floodplain, and stability and water mass conservation in the study area were essential to ensuring the accuracy of the simulation results. Uchiyama (2004) developed a simple formulation for a wetting or drying scheme that could selectively retain computational robustness and water mass conservation in the domain. Therefore, in this study, the method proposed by Uchiyama (2004) was applied to each wetting or drying cell. In this method, the total local depth is used to define the wetting or drying mesh, and a land mask function (*LMF*) is applied. *LMF*=1 indicates that the cell is considered "wet," whereas *LMF*=0 indicates that the cell is "land." Recalculation is performed for all cells after each time step. A threshold depth value d_{th} and a minimum depth d_{min} are defined in the previous step, and the total depth of water $D(m,n)=h(m,n)+\eta(m,n)$ at each cell (m,n) is compared with d_{th}. If the $D(m,n)$ value is greater than or equal to d_{th}, LMF(m,n) is set to 1. Otherwise, the three conditions below are immediately applied:

$$\left.\begin{aligned}&\min\left[\eta_{m-1,n},\eta_{m+1,n},\eta_{m,n-1},\eta_{m,n+1}\right]\le\eta_{m,n}\\&\min\left[D_{m-1,n},D_{m+1,n},D_{m,n-1},D_{m,n+1}\right]\le d_{th}\\&\max\left[LMF_{m-1,n},LMF_{m+1,n},LMF_{m,n-1},LMF_{m,n+1}\right]=0\end{aligned}\right\} \quad (5)$$

If at least one of these conditions is satisfied, *LMF*(m,n) is set to 0. This means that the cell is dry. If none of the above conditions are satisfied, the total

depth $D(m,n)$ of water at each cell (m,n) is compared with d_{min}. If the $D(m,n)$ value is less than or equal to d_{min}, $LMF(m,n)$ is set to 0. Otherwise, $LMF(m,n)$ is set to 1.

In previous research, an optimal operation procedure for the Van Coc Lake to protect Hanoi from the Red River flood disaster for the largest recorded flood, which occurred between the 16th and 27th of August 1971 was proposed by Anh *et al.* (2020a). In the optimal operation procedure, the inflow discharge into the Van Coc Lake and outflow discharge at the Day Weir were determined to maximize the flood mitigation function of the Van Coc Lake. In addition, the calculated water level at the Day Weir was recorded for the optimal operation procedure. In this study, the water level at the Day Weir was used as the input boundary condition, and because of the emergency situation, the Day Weir was fully opened. Figure 2 shows an important moment when floodwater from the Van Coc Lake reached the Day Weir. This point in time, denoted Time–0, was used for the movement of floodwater in the analysis scenarios considered in this study. The discharge observed during the catastrophic flood that occurred between the 16th and 27th of August 1971 was used for the inflow boundary condition at the Tich–Bui Rivers. In general, the boundary conditions for 2–D models include upstream and downstream boundary conditions that are often specified as an upstream flow rate or water level and a downstream water level (Horritt and Bates, 2002; Dutta *et al.*, 2007; Q. Liu *et al.*, 2014; An *et al.*, 2015). Values for these can often be established from historical hydrologic records. However, in many cases in which historical hydrological data are limited, the boundary conditions are established assuming uniform flow (Pappenberger *et al.*, 2006; Sun *et al.*, 2008; González–Sanchis *et al.*, 2012). In this study, uniform flow was assumed for the downstream end boundary condition.

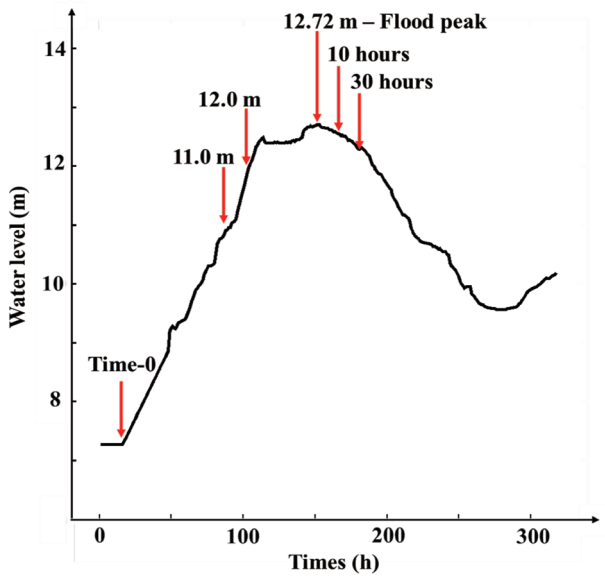

Fig. 2. Input water level for the boundary condition at the Day Weir and the times of flood impact assessment when the floodwater level reached 11.0 m, 12.0 m, and 12.72 m (the flood peak) at the Day Weir and at 10 and 30 h after the flood peak.

Figure 2 shows the input water level at the Day Weir and flood impact assessment times. The ground elevation of the Day Weir is 9.0 m, and the dike crest elevation is approximately 16.0 m. The impact of floodwater on the residential areas within the floodplain was calculated and analyzed at the times when the floodwater level reached 11.0 m, 12.0 m, and 12.72 m (the flood peak) at the Day Weir and at 10 and 30 h after the flood peak.

RESULTS AND DISCUSSION

Inundated areas and Flood risk mapping

Figure 3 shows the distribution of the inundation depth, and Fig. 4 shows the inundated residential areas and their proportions to the total residential area in each zone when the floodwater reached 11.0 m at the Day Weir. In this study, degrees of inundation were classified into five levels, A, B, C, D, and E, to represent flood risk levels. The water depth ranges corresponding to inundation levels A, B, C, D, and E were taken to be 0.5 to 1.0 m, 1.0 to 2.0 m, 2.0 to 3.0 m, 3.0 to 4.0 m, and more than 4.0 m, respectively. In Zone 1, 30.33% (3.43 km^2) of the residential areas, a total area of 11.31 km^2, was inundated. The areas inundated at depth levels A and B made up 11.85% (1.34 km^2) and 9.2% (1.04 km^2) of the residential areas, respectively. In Zone 2, 18.86% (7.66 km^2) of the residential areas were inundated. The areas inundated at depth levels A and B made up 9.97% (4.05 km^2) and 6.40% (2.60 km^2) of the residential areas. The most dangerous inundation depth levels, D and E, accounted for 0.54% (0.22 km^2) and 0.12% (0.05 km^2), respectively. Zone 3 has a total residential area of 13.50 km^2, and 28.69% (3.87km^2) of that area was calculated to be inundated. Inundation depth levels A and B accounted for 9.94% (1.34 km^2) and 13.05% (1.76 km^2), respectively.

Time–0 was an important point of reference for when floodwater from the Van Coc Lake reached the Day Weir. The floodwater reached a height of 11.0 m at the Day Weir 75 h after Time–0. Floodwater was mainly concentrated around the Day River from the north to the south, and some areas located in the southwest of Zone 1 were severely inundated. Most of the residential areas in Zone 1 were not affected by floodwater when the floodwater reached 11.0 m at the Day Weir. The variation in the inundation depth was wide, possibly because there was a significant elevation difference between the river bottom and the floodplain areas. In Zone 2, the floodwater began to spread out from the Day River and the Tich–Bui rivers as well. Some of the residential areas located in the center of the Zone 2 were heavily inundated. However, most of the residential areas located in the west were not affected by floodwater. In Zone 3, because of the increase in inundation depth, a larger proportion of the residential areas were inundated. The areas located in the southwest were affected by floodwater first because of the lower elevation, and these areas was the second most heavily impacted by flooding, compared with Zones 1 and 2. Obviously, the residential areas in each zone mainly experienced inun-

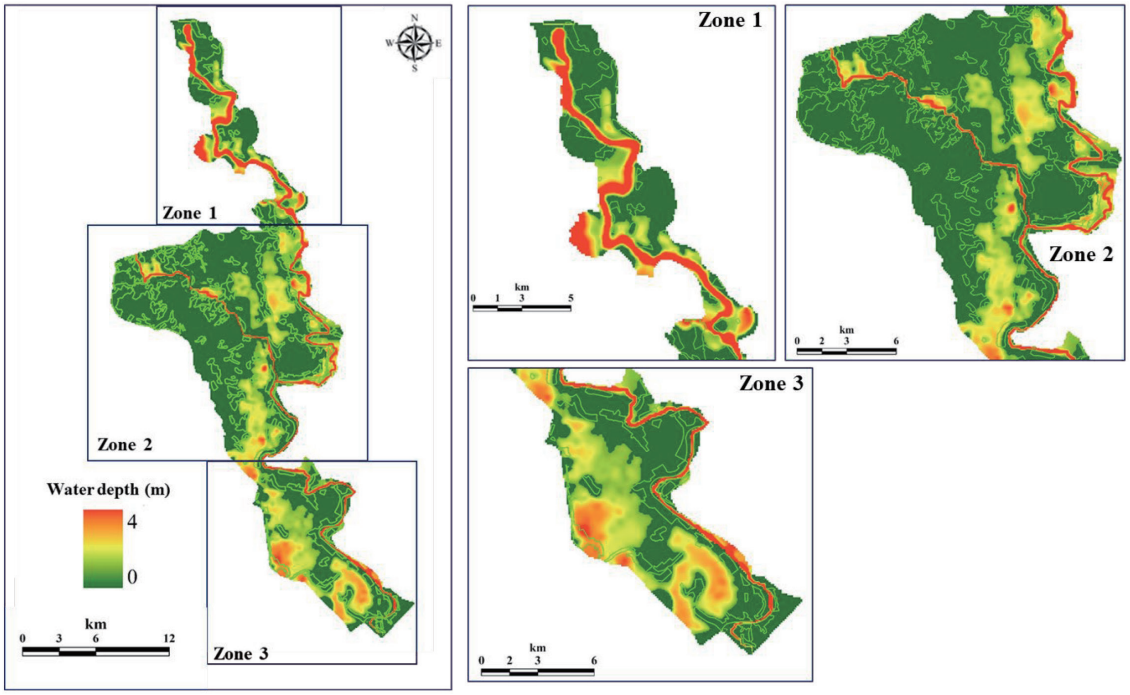

Fig. 3. Inundation depth distribution in the study area when the floodwater level at the Day Weir reached 11.0 m.

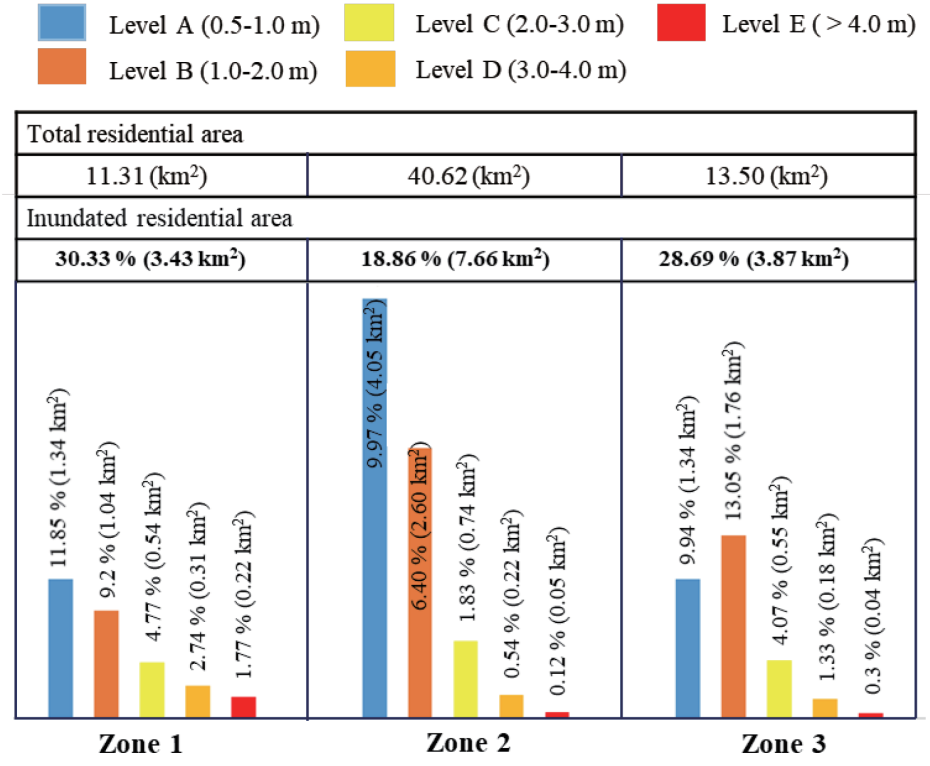

Fig. 4. Inundated residential areas and their percentages of the total residential area in each zone when the floodwater level reached 11.0 m at the Day Weir.

dation depth levels A and B. The results clearly show that floodwater began to impact 30% of the residential areas when the floodwater reached 11.0 m at the Day Weir.

Figures 5 and 6 illustrate the distribution of the inundation depth and the inundated residential areas and their proportions of the total residential areas in each zone when the floodwater reached 12.0 m at the Day Weir. In Zone 1, 57.65% (6.52 km^2) of the residential areas were inundated, with 19.89% (2.25 km^2) and 23.25% (2.63 km^2) inundated to depth levels A and B, respectively. In Zone 2, 26.59% (10.80 km^2) of the residential areas were inundated, with 11.15% (4.53 km^2) and 11.47% (4.66 km^2) inundated to depth levels A and

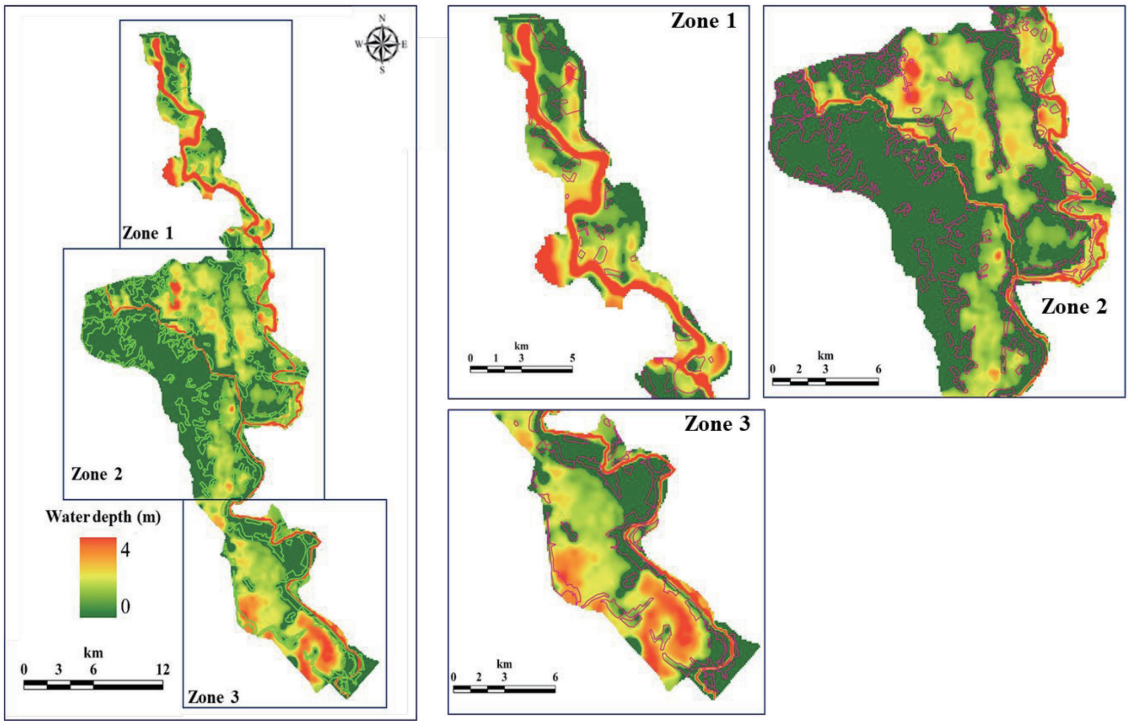

Fig. 5. Inundation depth distribution in the study area when the floodwater level at the Day Weir reached 12.0 m.

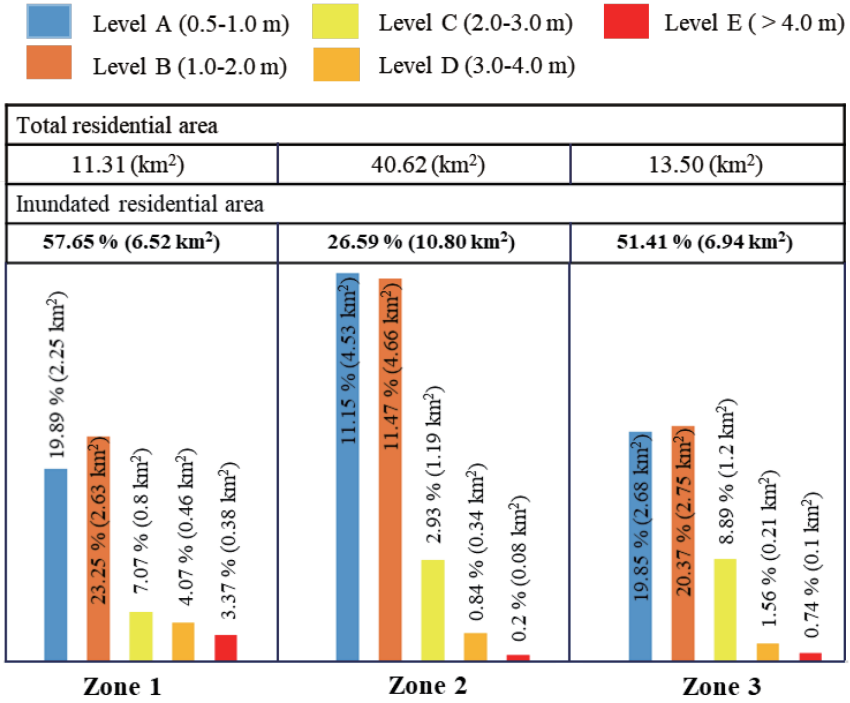

Fig. 6. Inundated residential areas and their percentage to the total residential area in each Zone when the floodwater level reached 12.0 m at the Day Weir.

B, respectively. The areas of Zone 2 corresponding to depth levels C, D, and E were 2.93% (1.19 km^2), 0.84% (0.34 km^2), and 0.20% (0.08 km^2), respectively. In Zone 3, more than 50% of the residential area was inundated. The most severely inundated residential areas, i.e., inundation depth levels D and E, accounted for 1.56% (0.21 km^2) and 0.74% (0.1 km^2), respectively. The areas in Zone 3 inundated to depth levels A, B, and C made up 19.85% (2.68 km^2), 20.37% (2.75 km^2), and 8.89% (1.2 km^2), respectively.

The simulation results indicate that the floodwater required 87 h from Time–0 to reach 12.0 m at the Day Weir, with only 12 h required to rise from 11.0 m to 12.0 m. Many of the residential areas were inundated to a depth of less than 0.5 m. In Zone 1, the floodwater spread out and affected the residential areas severely,

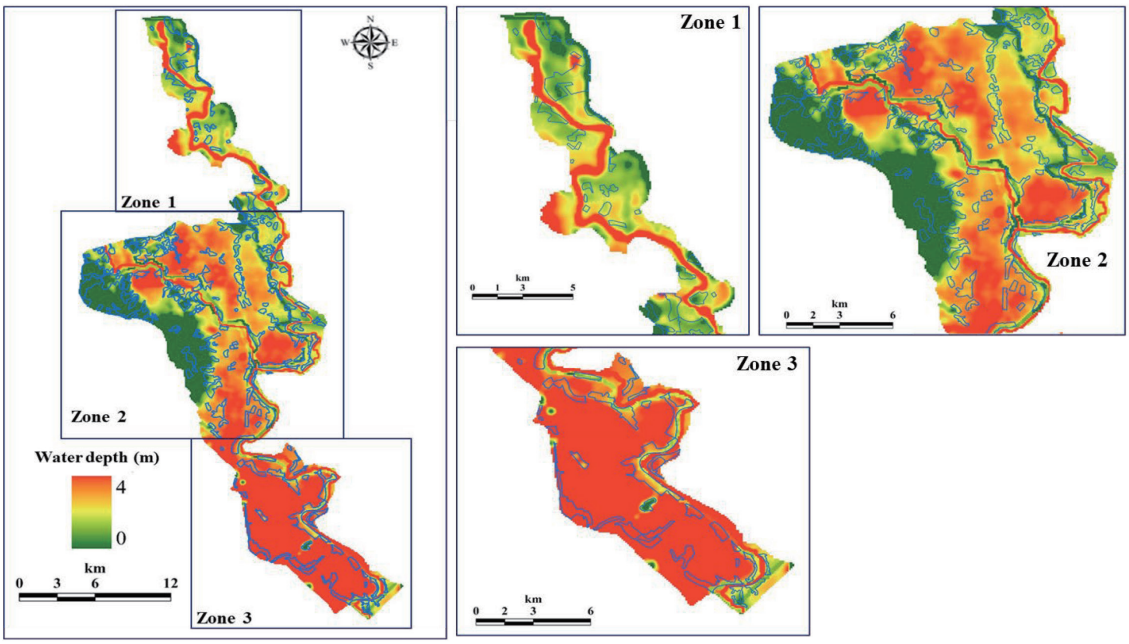

Fig. 7. Inundation depth distribution in the study area when the floodwater level at the Day Weir reached 12.72 m.

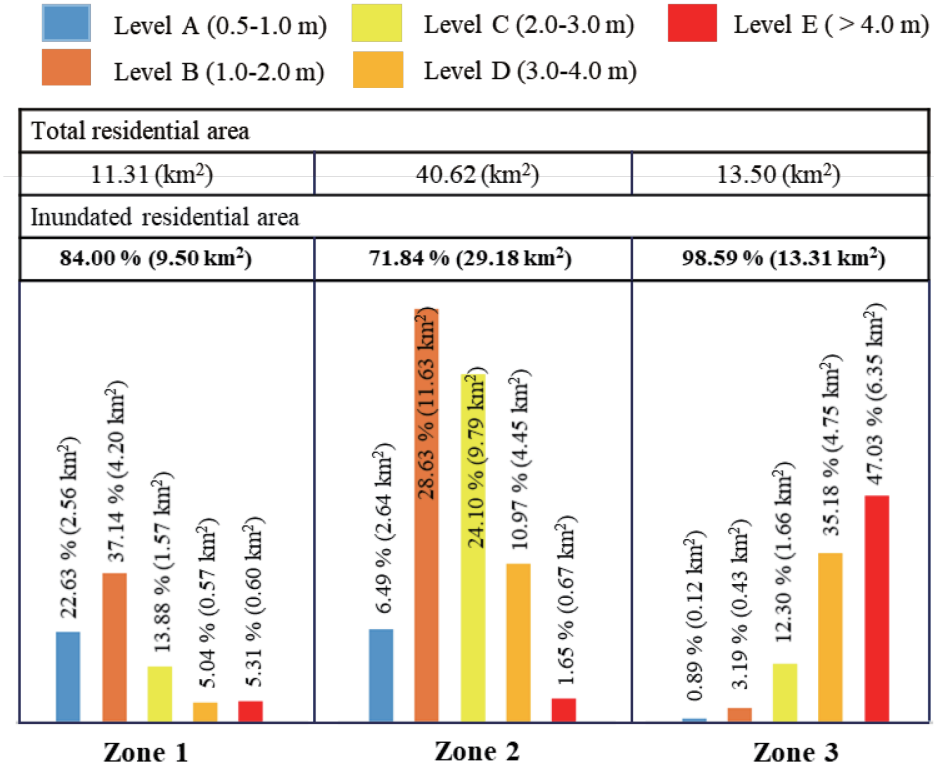

Fig. 8. Inundated residential areas and their percentages of the total residential area in each zone when the floodwater level reached 12.72 m at the Day Weir.

particularly those at low elevations near the riverbed. In Zone 2, the residential areas on the northeast and southeast sides were significantly affected by flooding, while residential areas on the southwest side were not impacted, because they are located at higher elevations. In Zone 3, the low–elevation areas in the southeast were heavily influenced by floodwater, and the inundated residential areas were mainly concentrated on the southeast side. In summary, most of the residential areas were inundated to depth levels A, B, or C when the floodwater reached 12.0 m at the Day Weir. The percentage of affected residential areas located in Zones 1 and 3 increased by 20% when the floodwater reached 11.0 m at the Day Weir.

Figures 7 and 8 illustrated the distributions of the inundation depth and the inundated residential areas

and their proportions of the total residential areas in each zone when the floodwater reached the flood peak at 12.72 m. Most of the residential areas in the study area were heavily inundated. In Zone 1, 84.00% (9.50 km^2) of the residential areas were inundated. The proportions of areas reaching inundation depth levels A and B were 22.63% (2.56 km^2) and 37.14% (4.20 km^2), respectively. In Zone 2, the residential areas were mainly inundated to depths from 1.0 to 3.0 m and were located in the southeast and northeast. In this zone, 71.84% (29.18 km^2) of the total area was inundated. The proportions of areas in Zone 2 reaching inundation depth levels B and C were 28.63% (11.63 km^2) and 24.10% (9.79 km^2), respectively. In Zone 3, most of the residential areas in the study area were inundated to depths of more than 4.0 m. This can be explained by the lower elevations at which these residential areas are located. As shown in Figs. 7 and 8, 98.59% (13.31 km^2) of the residential areas in Zone 3 were inundated, and the areas inundated to depth levels D and E made up 35.18% (4.75 km^2) and 47.03% (6.35 km^2) of the total area of the zone.

The simulation results indicate that the floodwater required 135 h from Time–0 to reach the flood peak of 12.72 m at the Day Weir, 48 h of which corresponded to the increase from 12.0 m to 12.72 m, as a result of the slow movement of floodwater when most of the floodplain areas were filled. The inundation depth levels of the Day River system when the floodwater reached the flood peak of 12.72 m provide a strong warning about the dangers of floodwater throughout the study area. In Zone 1, the residential areas near the riverbed and many residential areas located at low elevations were severely inundated. However, most of the inundated residential areas were inundated to depths of less than 2 m because they are located at higher elevations. In Zone 2, the residential areas located to the southwest were unaffected. Unfortunately, the remaining residential areas in this zone were severely affected by floodwater. In Zone 3, floodwater significantly impacted the residential areas because of their low elevation. In summary, floodwater is a dangerous natural hazard that threatens residential areas throughout the study area.

Figures 9 and 10 show the simulation results for the inundated residential areas 10 h after the flood peak. In Zone 1, 83.73% (9.47km^2) of the residential areas were inundated at that time, which is a slightly lower percentage than that at the flood peak time. The proportions of areas that were flooded to inundation depth levels A and B were 26.08% (2.95 km^2) and 34.66% (3.92 km^2). In addition, although the percentages of the areas that were flooded to inundation depths C, D, and E were slightly smaller than those at the flood peak time, they were still high. In Zone 2, there was an increase in the percentage of inundated residential areas, to 71.84% (29.18 km^2), compared to that at the flood peak time. The floodwater began to spread out to the residential areas located in the southwest. The percentage of the residential areas that reached inundation depth level E was 4.56% (1.85 km^2), and most of the residential areas were flooded to depths from 1.0 to 4.0 m. More seriously, in Zone 3, 63.78% (8.61 km^2) of the residential areas were inundated to depths of more than 4.0 m. The proportions of the areas flooded to inundation depth levels A, B, C, and D were 0.74% (0.10 km^2), 1.93% (0.26 km^2), 6.22% (0.84 km^2), and 26.59% (3.59 km^2).

After the flood peak, the water level at the Day Weir decreased while the floodwater levels were still increasing in the downstream areas. This is the time period

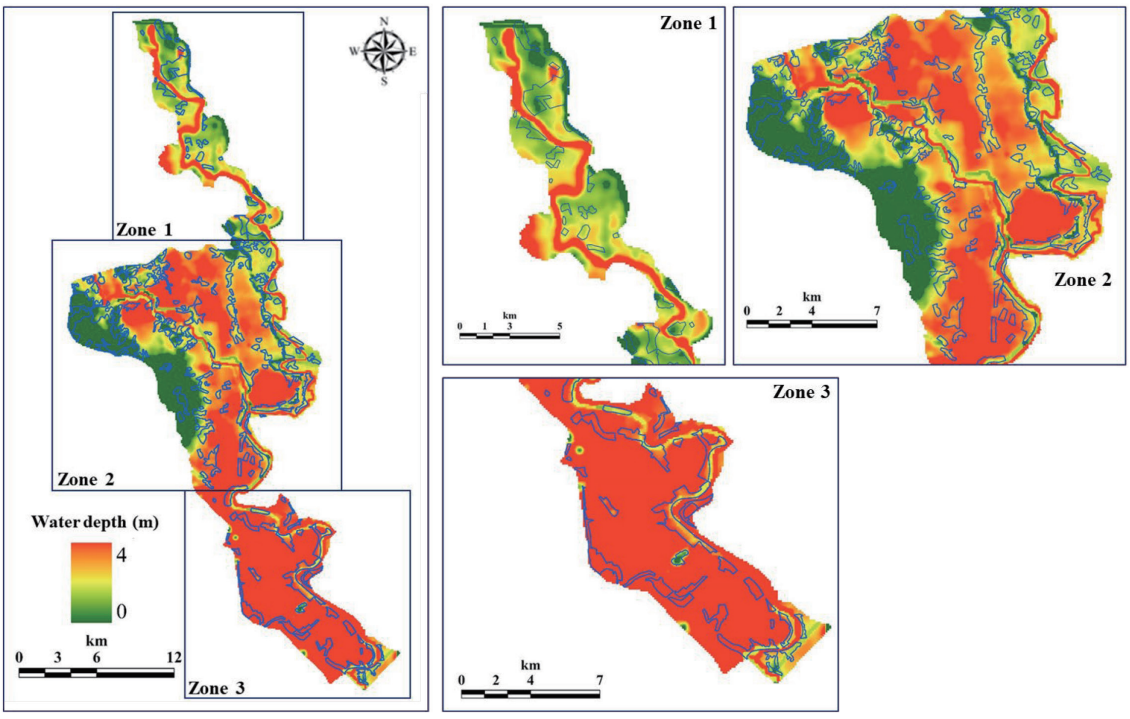

Fig. 9. Inundation depth distribution in the study area 10 h after the flood peak.

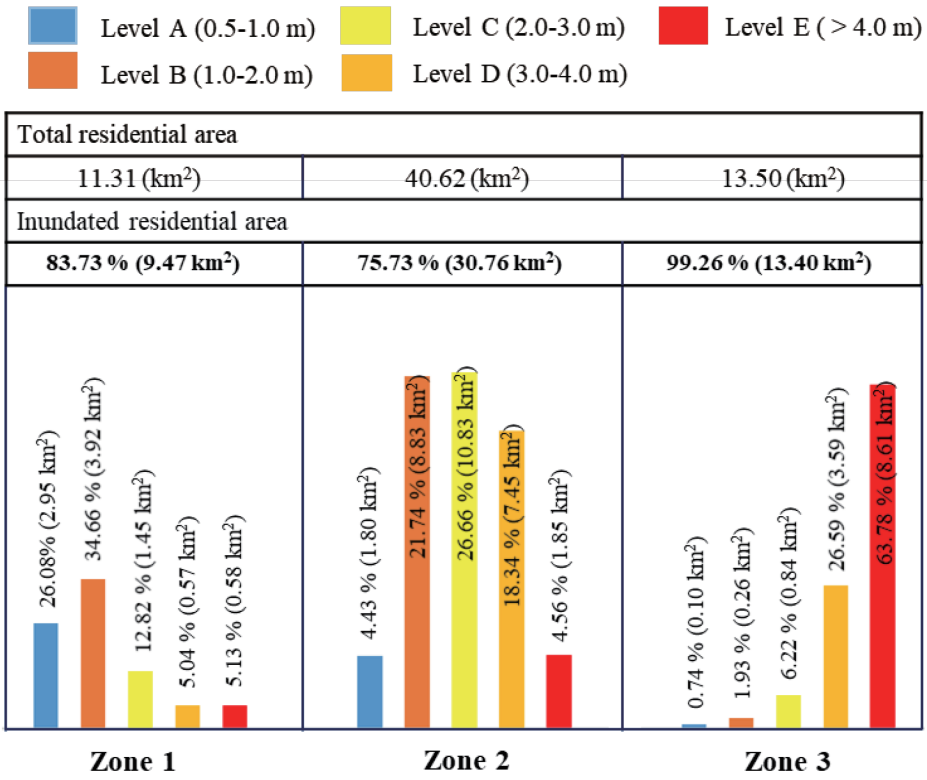

Fig. 10. Inundated residential areas and their percentages of the total residential area in each zone 10 h after the flood peak.

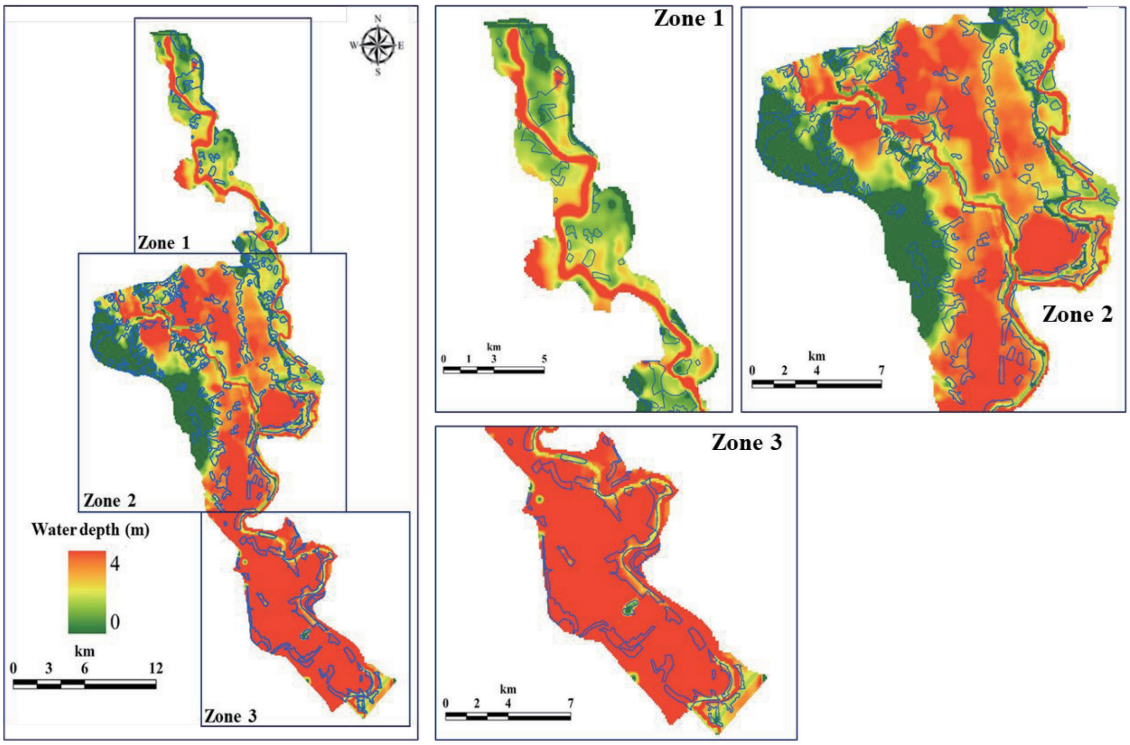

Fig. 11. Inundation depth distribution in the study area 30 h after the flood peak.

during which residential areas were considered to be most affected by the floodwater throughout the study area. The simulation results indicate that after the flood peak time, floodwater continued to spread throughout Zones 2 and 3 and that 10 h after the flood peak, the residential areas were inundated to depths primarily less than 2.0 m in Zone 1, primarily to depths from 1.0 to 4.0 m in Zone 2, and primarily to depths greater than 4.0 m in Zone 3.

Figure 11 shows the distribution of the inundation

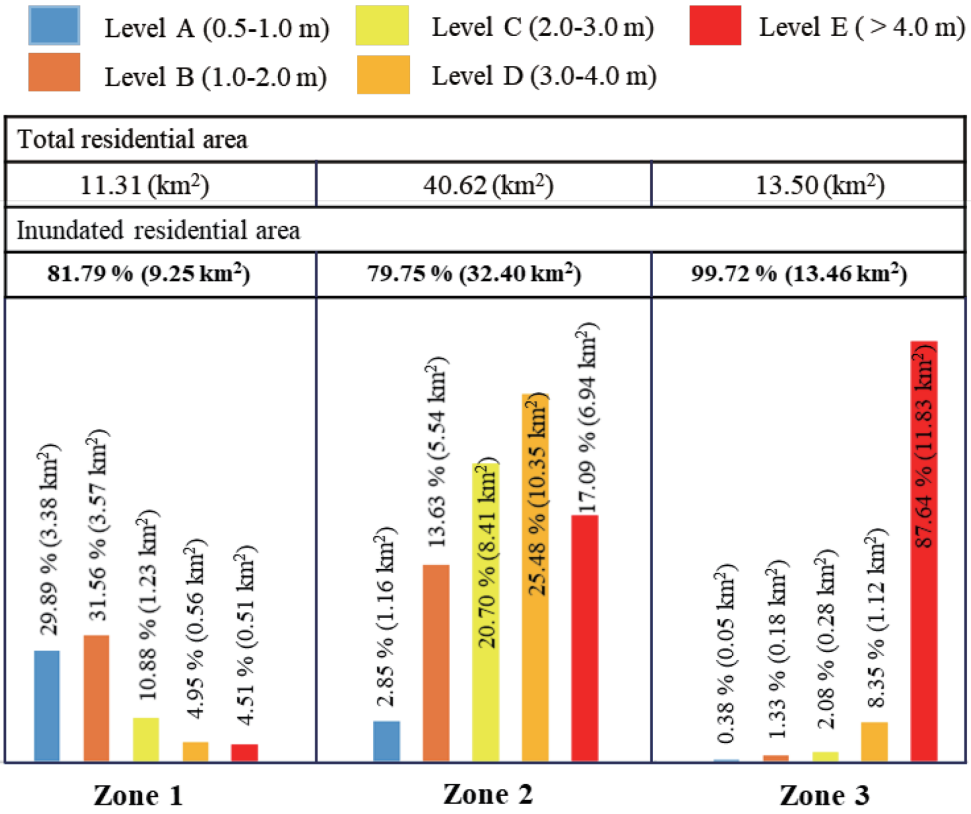

Fig. 12. Inundated residential areas and their percentages of the total residential area in each zone 30 h after the flood peak.

depths in each zone 30 h after the flood peak, and Fig. 12 shows the inundated residential areas and their proportions of the total residential area at that time. In Zone 1, the percentage of inundated residential areas decreased slightly in comparison to that at 10 h after the flood peak, because of the decrease in the water level at the Day Weir. The floodwater was mainly concentrated around the Day River, with 81.79% (9.25 km^2) of the residential areas inundated, most of them to depths of 0.5 to 2.0 m. In Zone 2, the residential areas located in the center were inundated more heavily as the floodwater spread out strongly from the Day River and the Tich–Bui rivers. However, most of the residential areas located in the west were not affected by floodwaters because they were located at higher elevations. In this zone, 79.75% (32.40 km^2) of the residential areas were inundated. Areas inundated to the most dangerous depth level, E, accounted for 17.09% (6.94 km^2). Areas inundated to depth levels C and D also accounted for high proportions: 20.70% (8.41 km^2) and 25.48% (10.35 km^2), respectively. In Zone 3, the flooding conditions constituted a disaster, with 99.72% (13.46 km^2) of the residential areas inundated, 87.64% (11.83 km^2) of them to depths of more than 4.0 m. Areas inundated to depth levels A, B, C, and D only made up small proportions of the total area.

The time point 30 h after the flood peak was selected to demonstrate the danger of the hazard levels in the floodplains of the study area after the flood peak, especially in the residential areas. The residential areas located at the lowest elevations at the downstream end of the study area were most strongly impacted by floodwater. The hazard zonation map in Fig. 11 shows how seriously the three zones of the floodplains in the study area were flooded when the optimal operation procedure for the Van Coc Lake was applied.

In summary, Time–0 was an important moment when floodwater from the Van Coc Lake reached the Day Weir, and from that moment in time onward, the floodwater needed 75, 87, and 135 h to reach depths of 11.0 m, 12.0 m, and the flood peak at 12.72 m, respectively, at the Day Weir. Only 75 h were required for the floodwater depth to reach a sufficiently dangerous level to have a serious impact on many residential areas, and the increase in floodwater depth from 11.0 m to 12.0 m occurred particularly rapidly. The simulation results yielded reliable flood susceptibility maps that identify the areas that were most impacted by floodwater. When the floodwater reached 11.0 m at the Day Weir, there 30.33% (3.43 km^2) of the residential areas in Zone 1, 18.86% (7.66 km^2) of those in Zone 2, and 28.69% (3.87 km^2) of those in Zone 3 were inundated. The flood situation became more serious when the floodwater depth reached 12.0 m at the Day Weir, with 57.65% (6.52 km^2), 26.59% (10.80 km^2), and 51.41% (6.94 km^2) of the residential areas in Zones 1, 2, and 3, respectively, being inundated. However, the results also indicate that the majority of the residential areas were inundated to depths of 0.5 to 2.0 m at that time. When the floodwater reached 12.72 m (the flood peak) at the Day Weir, 84.00% (9.50 km^2) of the residential areas in Zone 1,

71.84% (29.18 km^2) of those in Zone 2, and 98.59% (13.31 km^2) of those in Zone 3 were inundated. Furthermore, because of the significant differences in elevation from the Day Weir to the downstream end of the study area, the proportions of inundated residential areas 10 and 30 h after the flood peak were significantly different in the different zones, with 83.73% (9.47 km^2) and 81.79% (9.25 km^2), respectively, inundated in Zone 1; 75.73% (30.76 km^2) and 79.75% (32.40 km^2), respectively, inundated in Zone 2; and 99.26% (13.40 km^2) and 99.72% (13.46 km^2), respectively, inundated in Zone 3.

CONCLUSIONS

The results of this study illustrate the influence of floodwater on residential areas along the Day River system during a flood peak period when the operating procedure for emergency situations for the Van Coc Lake and Day Weir proposed by Anh *et al*. (2020a) is applied. Reliable flood susceptibility maps have been developed based on the results, and the use of such maps is essential for preventing and reducing flood damage in the study area. A combination of a 2–D depth-integrated hydrodynamic model and the latest DEM was utilized in the simulation. A study area comprising grid cells with a 50–m resolution was used, and a wetting–and–drying scheme was utilized to identify the wet and dry areas at each time step.

To assess the impact of floodwater on the residential areas along the Day River system, the boundary conditions of the proposed operating procedure for emergency situations were utilized to define the input water level at the Day Weir. The impact of floodwater on residential areas was calculated for flood heights of 11.0, 12.0, and 12.72 m (flood peak) at the Day Weir and at 10 and 30 h after the flood peak. The results indicate that three zones of floodplains in the study area were flooded easily in the emergency situation considered. Most of the residential areas were at high risk of severe damage due to inundation when the floodwater reached 12.72 m at the Day Weir, and this risk persisted even 10 and 30 h after the flood peak. Exceptions to this were the residential areas southwest of Zone 2, which are located at a higher elevation. Approximately 30% of the residential areas were inundated when the floodwater reached 11.0 m at the Day Weir and mainly experienced inundation depth levels A and B. When the floodwater reached 12.0 m at the Day Weir, most of the residential areas were inundated to levels A, B, and C. At the flood peak, the floodwater depths were at dangerous levels for residential areas throughout the entire study area. Even 10 and 30 h after the flood peak, most of the residential areas were inundated to depths up to 2.0 m in Zone 1, from 1.0 to 4.0 m in Zone 2, and to more than 4.0 m in Zone 3. These results provide an overview of the flood hazards to residential areas in the study area and provide a basis for future land use planning and a reference for the design of risk–reduction strategies for the Day River system in the overall development planning of Hanoi.

AUTHOR CONTRIBUTIONS

S. H. ANH, T. TABATA, and K. HIRAMATSU designed the study and conducted field observations. L. V. SON contributed to the field observations. S. H. ANH wrote the draft of the manuscript. T. TABATA, K. HIRAMATSU, L. V. SON, and M. HARADA revised the manuscript. All authors approved the final version of the manuscript and agreed to be accountable for all aspects of the work, ensuring that questions related to the accuracy or integrity of any part of the work are appropriately investigated and resolved.

ACKNOWLEDGMENTS

The authors appreciate the funding support of JSPS KAKENHI Grant Numbers JP18H03968 and JP17K15347.

REFERENCES

AHA (ASEAN Coordinating Centre for Humanitarian Assistance on Disaster Management) & JICA (Japan International Cooperation Agency) 2015 Natural Disaster Risk Assessment and Area Business Continuity Plan Formulation for Industrial Agglomerated Areas in the ASEAN Region, 2013 to 2015. Country Report–Vietnam

Ahmadi, M. M., S.A. Ayyoubzadeh, M. M. Namin and J. M. V. Samani 2009 A 2D Numerical Depth–averaged Model for Unsteady Flow in Open Channel Bends, *J. Agr. Sci. Tech*, **11**, 457–468

An, H., S. Yu, G. Lee and Y. Kim 2015 Analysis of an open source quadtree grid shallow water flow solver for flood simulation, *Quat. Int*, **384**, 118–128. https://doi.org/10.1016/j.quaint.2015.01.032

Anh, S. H., T. Tabata, K. Hiramatsu and M. Harada 2020b Flood Hazard Assessment of Residential Areas Outside the Protected Area of the Red River Dike System in Hanoi, Vietnam, *JARQ–JPN AGR RES Q*. (Accepted)

Anh, S. H., T. Tabata, K. Hiramatsu, M. Harada and L. N. Chung 2020a An optimal scenario for the emergency solution to protect the Hanoi Capital from flood disaster of the Red River by using the Van Coc Lake, *J. Flood Risk Manag*. (Accepted)

Anh, S. H., T. Tabata, K. Hiramatsu, M. Harada and L.V Son 2019a Assessment of Floodwater Behavior in Van Coc Lake, Hanoi in Event of Emergency Situation, *JARQ–JPN AGR RES Q*, **53**(3), pp.181–190. DOI: 10.6090/jarq.53.181

Balzano, A. 1998 Evaluation of methods for numerical simulation of wetting and drying in shallow water flow models, *Coast. Eng. Balzanor Coast. Eng*, **34**, 83–107. https://doi.org/10.1016/S0378-3839(98)00015-5

Bellos, V. and G. Tsakiris 2015 Comparing Various Methods of Building Representation for 2D Flood Modelling In Built–Up Areas, *Water Resour. Manag*, **29**, 379–397. https://doi.org/10.1007/s11269-014-0702-3

Blumberg, A.F. and G.L. Mellor 1987 A Description of a Three-Dimensional Coastal Ocean Circulation Model

Brufau, P., P. García–Navarro and M. E. Vázquez-Cendón 2004 Zero mass error using unsteady wetting–drying conditions in shallow flows over dry irregular topography, *Int. J. Numer. Methods Fluids*, **45**, 1047–1082. https://doi.org/10.1002/fld.729

Casulli, V. and E. Cattani 1994 Stability, Accuracy and Efficiency of a Semi–Implicit Method for Three–Dimensional Shallow Water Flow, *Comput. Math. with Appl*, **27**, 99–112

Caviedes–Voullième, D., M. Morales–Hernández, I. López–Marijuan and P. García–Navarro 2014 Reconstruction of 2D river beds by appropriate interpolation of 1D cross-sectional information for flood simulation, *Environ. Model. Softw*., **61**, 206–228. https://doi.org/10.1016/j.envsoft.2014.07.016

Chacón Rebollo, T., F. Hecht, M. Gómez Mármol, G. Orzetti and S. Rubino 2014 Numerical approximation of the Smagorinsky turbulence model applied to the primitive equations of the ocean, *Math. Comput. Simul*, **99**, 54–70. https://doi.org/10.1016/j.matcom.2013.04.023

Costabile, P., C. Costanzo, G. De Lorenzo and F. Macchione 2020 Is local flood hazard assessment in urban areas significantly influenced by the physical complexity of the hydrodynamic inundation model?, *J. Hydrol.*, **580**, 124231. https://doi.org/10.1016/j.jhydrol.2019.124231

Dottori, F., P. Salamon, A. Bianchi, L. Alfieri, F. A. Hirpa and L. Feyen 2016 Development and evaluation of a framework for global flood hazard mapping, *Adv. Water Resour.*, **94**, 87–102. https://doi.org/10.1016/j.advwatres.2016.05.002

Dutta, D., J. Alam, K. Umeda, M. Hayashi and S. Hironaka 2007 A two–dimensional hydrodynamic model for flood inundation simulation: a case study in the lower Mekong river basin, *Hydrol. Process*, **21**, 1223–1237. https://doi.org/10.1002/hyp

Eini, M., H.S. Kaboli, M. Rashidian and H. Hedayat 2020 Hazard and vulnerability in urban flood risk mapping: Machine learning techniques and considering the role of urban districts, *Int. J. Disaster Risk Reduct*, **50**, 101687. https://doi.org/10.1016/j.ijdrr.2020.101687

El Kadi Abderrezzak, K., A. Paquier and E. Mignot 2009 Modelling flash flood propagation in urban areas using a two–dimensional numerical model, *Nat Hazards*, pp. 433–460. https://doi.org/10.1007/s11069-008-9300-0

European Commission 2007 Handbook on good practices for flood mapping in Europe. Available at:https://ec.europa.eu/environment/water/flood_risk/flood_atlas/pdf/handbook_goodpractice.pdf

Fleischmann, A., R. Paiva and W. Collischonn 2019 Can regional to continental river hydrodynamic models be locally relevant? A cross–scale comparison, *J. Hydrol*, X **3**, 100027. https://doi.org/10.1016/j.hydroa.2019.100027

González–Sanchis, M., J. Murillo, B. Latorre, F. Comín and P. García–Navarro 2012 Transient two–dimensional simulation of real flood events in a mediterranean floodplain, *J. Hydraul. Eng*, **138**, 629–641. https://doi.org/10.1061/(ASCE)HY.1943-7900.0000565

Guerriero, L., G. Ruzza, F. M. Guadagno and P. Revellino 2020 Flood hazard mapping incorporating multiple probability models, *J. Hydrol*, **587**, 125020. https://doi.org/10.1016/j.jhydrol.2020.125020

Gusain, A., M. P Mohanty, S. Ghosh, C. Chatterjee and S. Karmakar 2020 Capturing transformation of flood hazard over a large River Basin under changing climate using a top–down approach, *Sci. Total Environ*, **726**, 138600. https://doi.org/10.1016/j.scitotenv.2020.138600

Haque, M. M., O. Seidou, A. Mohammadian and A. Gado Djibo 2020 Development of a time–varying MODIS/ 2D hydrodynamic model relationship between water levels and flooded areas in the Inner Niger Delta, Mali, West Africa, *J. Hydrol. Reg. Stud*, **30**. https://doi.org/10.1016/j.ejrh.2020.100703

Horritt, M. and P. Bates 2002 Evaluation of 1D and 2D numerical models for predicting river flood inundation, *J. Hydrol*, **268**, 87–99. https://doi.org/10.5059/yukigoseikyokaishi.64.628

Hu, M., T. Sayama, X. Zhang, K. Tanaka, K. Takara and H. Yang 2017 Evaluation of low impact development approach for mitigating flood inundation at a watershed scale in China, *J. Environ. Manage*, **193**, 430–438. https://doi.org/10.1016/j.jenvman.2017.02.020

Hu, S. and S. C. Kot 1997 Numerical Model of Tides in Pearl River Estuary with Moving Boundary. *J. Hydraul. Eng*, **123**: 9404

Hussein, S., M. Abdelkareem, R. Hussein and M. Askalany 2019 Using remote sensing data for predicting potential areas to flash flood hazards and water resources, *Remote Sens. Appl. Soc. Environ*, **16**, 100254. https://doi.org/10.1016/j.rsase.2019.100254

Kang, S. and F. Sotiropoulos 2012 Numerical modeling of 3D turbulent free surface flow in natural waterways, *Adv. Water Resour*, **40**, 23–36. https://doi.org/10.1016/j.advwatres.2012.01.012

Leendertse, J. J. 1970 A Water–quality Simulation Model for Well–mixed Estuaries and Coastal Seas, Vol. 1, *Principles of Computation*, February, RM–6230–RC

Liang, D., B. Lin and R. A. Falconer 2007 Linking one– and two–dimensional models for free surface flows, *Proc. ICE – Water Manag*, **160**, 145–151. https://doi.org/10.1680/wama.2007.160.3.145

Lin, L. U., L. I. Yu–cheng, T. Bin and C. Bing 2008 Numerical Simulation of Turbulent Free Surface Flow, *J. Hydrodyn*, 414–423

Liu, Q., Y. Qin, Y. Zhang and Z. Li 2014 A coupled 1D–2D hydrodynamic model for flood simulation in flood detention basin, *Nat. Hazards*, **75**, 1303–1325. https://doi.org/10.1007/s11069-014-1373-3

Liu, X., A. Mohammadian and J. A. I Sedano 2014 A Well–Balanced 2–D Model for Dam–Break Flow with Wetting and Drying, *J. Fluid Flow, Heat Mass Transf*. https://doi.org/10.11159/jffhmt.2014.005

Liu, Z. and V. Merwade 2018 Accounting for model structure, parameter and input forcing uncertainty in flood inundation modeling using Bayesian model averaging, *J. Hydrol*, **565**, 138–149. https://doi.org/10.1016/j.jhydrol.2018.08.009

Marras, S., M. A. Kopera, E. M. Constantinescu, J. Suckale and F. X. Giraldo 2018 A residual–based shock capturing scheme for the continuous/discontinuous spectral element solution of the 2D shallow water equations, *Adv. Water Resour*, **114**, 45–63. https://doi.org/10.1016/j.advwatres.2018.02.003

Marsooli, R., P. M. Orton, N. Georgas and A. F. Blumberg 2016 Three–dimensional hydrodynamic modeling of coastal flood mitigation by wetlands, *Coast. Eng*, **111**, 83–94. https://doi.org/10.1016/j.coastaleng.2016.01.012

Maulik, R. and O. San 2016 Dynamic modeling of the horizontal eddy viscosity coefficient for quasigeostrophic ocean circulation problems, *J. Ocean Eng. Sci*, **1**, 300–324. https://doi.org/10.1016/j.joes.2016.08.002

Mignot, E., A. Paquier and S. Haider 2006 Modeling floods in a dense urban area using 2D shallow water equations, *J. Hydrol*, **327**, 186–199. https://doi.org/10.1016/j.jhydrol.2005.11.026

Ministry of Natural Resources and Environment (MONRE), *Climate Change, Sea Level Rise Scenarios for Vietnam*, Hanoi: Vietnam Publishing House of Natural Resources, Environment and Cartography, 2012

Mishra, K. and R. Sinha 2020 Flood risk assessment in the Kosi megafan using multi–criteria decision analysis: A hydro-geomorphic approach, *Geomorphology*, **350**, 106861. https://doi.org/10.1016/j.geomorph.2019.106861

National Research Council 2015 Tying Flood Insurance to Flood Risk for Low–Lying Structures in the Floodplain. Washington, DC, *The National Academies Press*, https://doi.org/10.17226/21720

Nkwunonwo, U. C., M. Whitworth and B. Baily 2020 A review of the current status of flood modeling for urban flood risk management in the developing countries, *Scientific African*, **00269**. DOI: 10.1016/j.sciaf.2020.e00269

NOAA (National Oceanic and Atmospheric Administration) National Weather Service Public 1993 NOAA's Top Global Weather, Water, and Climate Events of the 20. US National Oceanic and Atmospheric Administration

Nur, I. and K. K. Shrestha 2017 An Integrative Perspective on Community Vulnerability to Flooding in Cities of Developing Countries, *Procedia Eng*, **198** (9), pp. 958–967. DOI: 10.1016/j.proeng.2017.07.141

Ogato, G. S., A. Bantider, K. Abebe and D. Geneletti 2020 Geographic information system (GIS)-Based multicriteria analysis of flooding hazard and risk in Ambo Town and its watershed, West shoa zone, oromia regional State, Ethiopia, *J. Hydrol. Reg. Stud*, **27**, 100659. https://doi.org/10.1016/j.ejrh.2019.100659

Pappenberger, F., P. Matgen, K. J. Beven, J. B. Henry, L. Pfister and P. Fraipont 2006 Influence of uncertain boundary conditions and model structure on flood inundation predictions, *Adv. Water Resour*, **29**, 1430–1449. https://doi.org/10.1016/j.advwa-

tres.2005.11.012

Pham Van, C., E. Deleersnijder, D. Bousmar and S. Soares–Frazão 2014 Simulation of flow in compound open–channel using a discontinuous Galerkin finite–element method with Smagorinsky turbulence closure, *J. Hydro–Environment Res*, **8**, 396–409. https://doi.org/10.1016/j.jher.2014.04.002

Pinos, J. and L. Timbe 2019 Performance assessment of two-dimensional hydraulic models for generation of flood inundation maps in mountain river basins, *Water Sci. Eng*, **12**, 11–18. https://doi.org/10.1016/j.wse.2019.03.001

Rakowsky, N., A. Androsov, A. Fuchs, S. Harig, A. Immerz, S. Danilov, W. Hiller and J. Schröter 2013 Operational tsunami modelling with TsunAWI – Recent developments and applications, *Nat. Hazards Earth Syst. Sci*, **13**, 1629–1642. https://doi.org/10.5194/nhess-13-1629-2013

Rollason, E., L. J. Bracken, R. J. Hardy and A. R. G Large 2018 The importance of volunteered geographic information for the validation of flood inundation models, *J. Hydrol*, **562**, 267–280. https://doi.org/10.1016/j.jhydrol.2018.05.002

Rong, Y., T. Zhang, Y. Zheng, C. Hu, L. Peng and P. Feng 2020 Three–dimensional urban flood inundation simulation based on digital aerial photogrammetry, *J. Hydrol*, **584**, 124308. https://doi.org/10.1016/j.jhydrol.2019.124308

Shadmehri Toosi, A., S. Doulabian, E. Ghasemi Tousi, G. H. Calbimonte and S. Alaghmand 2020 Large–scale flood hazard assessment under climate change: A case study, *Ecol. Eng*, **147**, 105765. https://doi.org/10.1016/j.ecoleng.2020.105765

Singh, R. K., V. G. Kumar Villuri, S. Pasupuleti and R. Nune 2020 Hydrodynamic modeling for identifying flood vulnerability zones in lower Damodar river of eastern India, *Ain Shams Eng. J*, 1–12. https://doi.org/10.1016/j.asej.2020.01.011

Smagorinsky, J. 1963 General circulation experiments with the primitive equations. *Mon Weather Rev*, **91**, pp. 99–164

SUN, D. P., H. Xue, P. T Wang, R. L Lu and X.L. Liao 2008 2–D Numerical Simulation of Flooding Effects Caused by South–to–North Water Transfer Project, *J. Hydrodyn*, **20**, 662–667. https://doi.org/10.1016/S1001-6058(08)60110-9

Tejada–Martínez, A. E., C. E Grosch, A. E Gargett, J. A Polton, J. A. Smith and J. A. MacKinnon 2009 A hybrid spectral/finite–difference large–eddy simulator of turbulent processes in the upper ocean, *Ocean Model*, **30**, 115–142. https://doi.org/10.1016/j.ocemod.2009.06.008

Thapa, S., A. Shrestha, S. Lamichhane, R. Adhikari and D. Gautam 2020 Catchment-scale flood hazard mapping and flood vulnerability analysis of residential buildings: The case of Khando River in eastern Nepal, *J. Hydrol. Reg. Stud*, **30**, 100704. https://doi.org/10.1016/j.ejrh.2020.100704

The World Bank Group 2016 Methods in Flood Hazard and Risk Management **2**, 2–4

Uchiyama, Y. 2004 Modeling wetting and drying scheme based on an extended logarithmic law for a three–dimensional sigma–coordinate coastal ocean model *Rep. Port Airpt. Res. Inst*., **43**, pp. 3–21

Vietnamese Government (2005) *National Report on Disaster Reduction In Vietnam*. Available at: https://www.unisdr.org/2005/mdgs-drr/national-reports/Vietnam-report.pdf

Werren, G., E. Reynard, S. N. Lane and D. Balin 2016 Flood hazard assessment and mapping in semi-arid piedmont areas: a case study in Beni Mellal, Morocco, *Nat. Hazards*, **81**, 481–511. https://doi.org/10.1007/s11069-015-2092-0

Wu, W. and Q. Lin 2015 Advances in Water Resources A 3–D implicit finite–volume model of shallow water flows, *Adv. Water Resour*, **83**, 263–276. https://doi.org/10.1016/j.advwatres.2015.06.008